NEUROSCIENCE

# ZBTB21 suppresses CRE-mediated transcription to impair synaptic function in Down syndrome

**Muzhen Qiao[1]†, Qianwen Huang[1]†, Xin Wang[2,3]*, Jiahuai Han[1,3,4]***



**Down syndrome (DS) is the most common chromosomal disorder and a major cause of intellectual disability. The genetic etiology of DS is the extra copy of chromosome 21 (HSA21)–encoded genes; however, the contribution of specific HSA21 genes to DS pathogenesis remains largely unknown. Here, we identified ZBTB21, an HSA21-encoded zinc-finger protein, as a transcriptional repressor in the regulation of synaptic function. We found that normalization of the *Zbtb21* gene copy number in DS mice corrected deficits in cognitive performance, synaptic function, and gene expression. Moreover, we demonstrated that ZBTB21 binds to canonical cAMP-response element (CRE) DNA and that its binding to CRE could be competitive with CRE-binding factors such as CREB. ZBTB21 represses CRE-dependent gene expression and results in the negative regulation of synaptic plasticity, learning and memory. Together, our results identify ZBTB21 as a CRE-binding protein and repressor in cAMP-dependent gene regulation, contributing to cognitive defects in DS.**

## INTRODUCTION

Down syndrome (DS) is a congenital disorder in which individuals are born with extra or partial chromosome 21 (HSA21). The extra number of genetic components may result in a variety of health problems, including developmental retardation, intellectual disability, and increased risk of Alzheimer's disease (*1*, *2*). Although a variety of abnormalities may occur in people with DS, most DS individuals exhibit moderate to severe cognitive impairment, which affects their quality of life. More than 200 genes on chromosome 21 may exert direct or indirect effects on DS-related deficits (*3*, *4*); however, the contribution of specific HSA21 genes to DS pathogenesis remains largely unknown.

Synaptic dysfunction plays a notable role in the intellectual disability observed in individuals with DS (*5*–*8*). Synaptic abnormalities (*5*) are evident in both prenatal and postnatal DS brains (*6*, *9*, *10*), with an observed imbalance in excitatory and inhibitory synaptic transmission in the brains of both individuals with DS and DS model mice (*11*, *12*). Synaptic plasticity, essential for memory encoding in the brain, is widely recognized (*13*, *14*). In addition, defects in hippocampal long-term potentiation (LTP) have been detected in DS mouse models (*15*, *16*).

Transcriptional regulation is critical for synaptic plasticity and memory formation. In particular, the cyclic adenosine 3′,5′-mono phosphate (cAMP)–dependent transcription pathway plays a central role in neuronal plasticity and long-term memory formation (*17*–*19*). The cAMP-dependent pathway has been found to function as a molecular switch to convert short- to long-term memory (*20*, *21*). cAMP response element–binding protein (CREB) is a key factor that regulates the transcription of multiple synapse-related genes by binding to cAMP-responsive elements (CREs) that occur either as a palindrome (TGACGTCA) or a half site (CGTCA/TGACG) in their promoters (*22*). The CREB protein is activated by the phosphorylation of protein kinase A at serine 133, further recruiting the coactivator CREB-binding protein (CBP) and its homolog p300. The recruitment of CBP/p300 is necessary for transcriptional activation. In addition to acting as coactivators, CBP and p300 are histone acetyltransferases that can also modulate histone acetylation (*23*). CBP/p300-targeted histone acetylation (H3K18 and H3K27) (*24*) is essential for CREB-dependent transcriptional pathways (*25*). CREB-mediated transcription provides a critical mechanism for regulating synaptic function, and defective cAMP-dependent transcription in DS mouse brains could contribute to DS-associated cognitive deficits (*26*).

Zinc finger (ZF) and broad-complex, tramtrack and bric-à-brac (BTB) domain–containing protein 21 (ZBTB21 or ZBT21) is a chromosome 21–encoded protein that may play a role in transcriptional regulation via the ZF domain as a DNA binding motif (*27*, *28*). ZBTB21 has been reported to be involved in a number of physiological and disease conditions, including early embryonic development (*29*), muscle development (*30*), and cancer (*31*). *ZBTB21* is located within the DS critical region (DSCR) and is potentially associated with congenital heart defects in DS (*32*). ZBTB21 is highly expressed in brain tissues, but its roles in learning and cognition and DS pathogenesis have not been elucidated.

Here, we demonstrated a role for chromosome 21–encoded ZBTB21 in DS-associated synaptic dysfunction. Our study showed that ZBTB21 competes with CRE motif binding with CREB and CBP/P300-mediated histone acetylation, leading to CRE-mediated transcriptional inhibition. Normalization of the *Zbtb21* gene copy number in DS mice corrected CRE-dependent gene expression and restored synaptic function. Furthermore, conditional overexpression of ZBTB21 in neurons results in synaptic and cognitive deficits in *Zbtb21* transgenic mice. In summary, our study identified ZBTB21 as a previously unknown transcriptional repressor of CRE-dependent gene expression and a pathogenic factor that disrupts synaptic function and cognitive performance in DS.

[1]State Key Laboratory of Cellular Stress Biology, School of Life Sciences, Faculty of Medicine and Life Sciences, Xiamen University, Xiamen, Fujian, 361102, China. [2]State Key Laboratory of Cellular Stress Biology, Fujian Provincial Key Laboratory of Neurodegenerative Disease and Aging Research, Institute of Neuroscience, Department of Neurology, the First Affiliated Hospital of Xiamen University, School of Medicine, Xiamen University, Xiamen, Fujian 361002, China. [3]Laboratory Animal Center, Faculty of Medicine and Life Sciences, Xiamen University, Xiamen, Fujian, 361102, China. [4]Research Unit of Cellular Stress of CAMS, Xiang'an Hospital of Xiamen University, Cancer Research Center of Xiamen University, School of Medicine, Faculty of Medicine and Life Sciences, Xiamen University, Xiamen, Fujian, 361102, China.
*Corresponding author. Email: wangx@xmu.edu.cn (X.W.); jhan@xmu.edu.cn (J.H.)
†These authors contributed equally to this work.

## RESULTS

### ZBTB21 acts as a cAMP response element-dependent transcriptional repressor

To identify previously unknown CRE-binding proteins, we transfected human embryonic kidney (HEK) 293T cells with biotin-labeled, CRE-containing double-stranded DNA fragments. Following transfection, we performed a pull-down assay followed by quantitative mass spectrometry (MS) analysis (Fig. 1A). The top 10 proteins enriched in biotin-CRE DNA pull-down are listed in Fig. 1B, and their MS ion intensities are shown in fig. S1A. As expected, known CRE-binding proteins such as CREB, activating transcription factor 1 (ATF1), and cAMP responsive element modulator were identified. The detection of c-Jun, JunB, and JunD may be attributed to the leucine zipper region in CREB, which is known for its role in forming homodimers or heterodimers with other proteins that have basic leucine zipper domains, including components of activator protein (AP)-1. Notably, ZBTB21, a previously unrecognized CRE-binding protein, was also identified (Fig. 1B). The specific interaction between the biotin-labeled CRE DNA fragment and ZBTB21 was further confirmed by the observation that ZBTB21 was pulled down by biotin-CRE but not by AP-1 (Fig. 1, C and D).

To determine whether ZBTB21 specifically regulates CRE-mediated gene transcription, we analyzed the transcriptional regulatory function of ZBTB21 using a CRE reporter. In HEK293T cells expressing CRE promoter-luciferase construct, ZBTB21 overexpression markedly reduced forskolin (FSK)-induced luciferase activity (Fig. 1E). However, ZBTB21 failed to regulate the expression of tumor necrosis factor (TNF)–induced nuclear factor κB (NF-κB)–driven luciferase (Fig. 1F), indicating that ZBTB21 selectively inhibits CRE-dependent transcription. Furthermore, the knockout (KO) of *ZBTB21* in HEK293T cells markedly increased FSK-induced CRE-dependent gene transcription (Fig. 1, G and H). This enhancement in gene transcription in *ZBTB21* KO cells was eliminated by restoring ZBTB21 expression (Fig. 1I). It needs to be noted that two splicing variants of *ZBTB21* exist (fig. S1B), and we used the cDNA of the long *ZBTB21* variant to restore the expression of ZBTB21 (Fig. 1I). This cDNA led to splicing, as evidenced by the detection of two bands in Western blotting (fig. S1C). When the cDNA of short-form *ZBTB21* was used (fig. S1C), it effectively suppressed CRE-dependent gene expression (fig. S1D). Although there was a noticeable trend indicating reduced cAMP and cAMP-dependent protein kinase (PKA) activity in $ZBTB21^{-/-}$ cells, this difference did not achieve statistical significance. Furthermore, our investigations revealed that overexpression of ZBTB21 did not alter cAMP levels or PKA activity (fig. S1E). Collectively, our findings demonstrate that ZBTB21 acts to suppress CRE-dependent transcription.

CREB is the most studied CRE-binding protein, and we determined that the interaction of ZBTB21 with CRE did not require the presence of CREB (fig. S1F). We subsequently tested whether ZBTB21 could compete with the binding of CREB to the CRE element using coexpression and pull-down assays and found that ZBTB21 could compete with the binding of CREB or ATF1 to the CRE (Fig. 2A and fig. S1G). Similarly, an electrophoretic mobility shift assay (EMSA) showed an efficient shift of the CRE DNA fragment by CREB, and ZBTB21 dose-dependently reduced the shifted CRE DNA (Fig. 2B). However, the binding of ZBTB21 to the CRE element could not be detected as a uniform band in the EMSA (Fig. 2B).

Epigenetic modification of CBP/P300 plays a critical role in CRE-mediated transcription. To determine whether ZBTB21 regulates CRE-mediated transcription through epigenetic alterations, we infected mouse primary neurons with lenti-*Zbtb21* (*ZBTB21-OE*) and analyzed the genome-wide DNA binding patterns of H3K27ac through cleavage under target and tagmentation sequencing (CUT&Tag-seq) (fig. S1H) (*33*). Our findings revealed that, compared to the control group, the ZBTB21 overexpression group exhibited a significantly reduced signal intensity of H3K27ac at gene peaks located in the transcription start site (TSS) regions [$P$ value < 0.05, $|\log_2$ fold change$| > 1$] (Fig. 2C). Furthermore, Gene Ontology (GO) and Kyoto Encyclopedia of Genes and Genomes pathway enrichment analysis revealed that genes with altered H3K27ac regions highlighted associations with synaptic function, learning and memory, and cAMP-mediated signaling pathways (Fig. 2D).

To determine the functional domains essential for suppressing CRE-mediated transcription, we generated different truncated ZBTB21 constructs and examined their effects on the expression of the CRE-luciferase reporter (Fig. 2, E to G). We found that the ZBTB21 ΔBTB and ZBTB21 ΔZF domains were less effective at suppressing CRE-luciferase activity than the full-length ZBTB21 domain (Fig. 2G), suggesting that the N-terminal BTB and ZF domains are required for the function of ZBTB21 as a CRE transcriptional repressor.

### Normalizing the *Zbtb21* copy number restores synaptic and cognitive deficits in Dp16 mice

To determine whether *Zbtb21* triplication contributes to DS pathogenesis, we generated wild-type (WT), $Zbtb21^{+/-}$, Dp16, and Dp16;$Zbtb21^{+/-}$ mice by breeding Dp16 mice with $Zbtb21^{+/-}$ mice (Fig. 3A). As expected, *Zbtb21* mRNA expression in Dp16 mice was higher than that in WT mice, and in Dp16;$Zbtb21^{+/-}$ mice, it was comparable to that in WT mice (Fig. 3B). To evaluate the cognitive performance of WT, $Zbtb21^{+/-}$, Dp16, and Dp16;$Zbtb21^{+/-}$ mice, we performed a series of behavioral tests and found that the learning and memory abilities of the Dp16 mice were impaired and that the cognitive deficits were largely restored in the Dp16;$Zbtb21^{+/-}$ mice (fig. S2A and Fig. 3, C to E). Notably, $Zbtb21^{-/-}$ mice exhibited normal learning and memory (fig. S2, B to D), suggesting that the effect of ZBTB21 on cognitive performance is more likely to be exclusively negative.

Given the key role of CREB in regulating synaptic plasticity, we performed electrophysiological recordings in the hippocampal CA1 region and found that Dp16 mice showed compromised LTP, and synaptic deficits were corrected in Dp16;$Zbtb21^{+/-}$ mice (Fig. 3, F and G). In addition, we noted that *Zbtb21* haploinsufficiency in Dp16; $Zbtb21^{+/-}$ mice corrected the abnormalities in basal synaptic transmission (Fig. 3H). Moreover, normalizing the *Zbtb21* copy number restored the frequency of spontaneous excitatory postsynaptic currents (sEPSCs) (Fig. 3I) but not the frequency of spontaneous inhibitory postsynaptic current (sIPSCs) (Fig. 3J) in the hippocampal CA1 pyramidal neurons of Dp16 mice. These findings collectively suggest that the disruption in the balance between excitation and inhibition (Fig. 3K) observed in the hippocampus of Dp16 mice can be ameliorated by *Zbtb21* haploinsufficiency, leading to the restoration of synaptic and cognitive function in Dp16;$Zbtb21^{+/-}$ mice.

Consistent with the electrophysiological results, we found that dendritic spine density was also restored in the hippocampus of Dp16;$Zbtb21^{+/-}$ mice, as revealed by Golgi staining (Fig. 3, L and

A

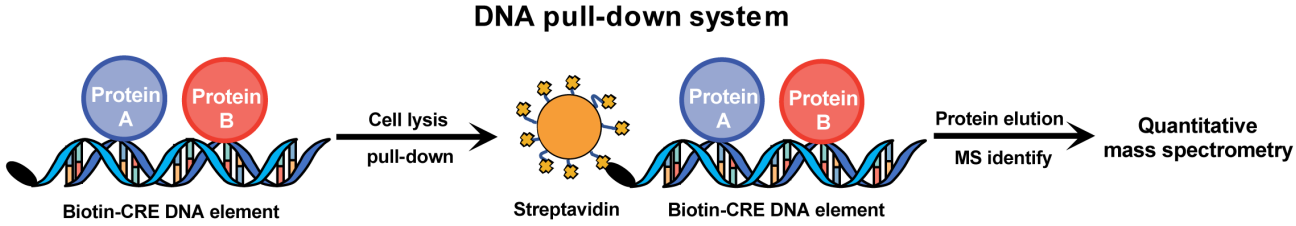


B

| Protein name | Peptide number | Background peptide intensity | Pull-down peptide intensity | Enrichment (fold) |
|---|---|---|---|---|
| ZBTB21 | 25 | 1663.58 | 394,297.00 | 237.02 |
| JUN | 21 | 1027.47 | 280,807.00 | 273.30 |
| ATF1 | 16 | 1158.94 | 239,944.00 | 207.04 |
| CREB1 | 14 | 1316.65 | 764,518.00 | 580.65 |
| ATF7 | 12 | 326.43 | 141,306.74 | 432.89 |
| JUNB | 4 | 1815.38 | 67,814.00 | 37.36 |
| JUND | 4 | 1248.00 | 152,111.06 | 121.88 |
| CREM | 4 | 730.13 | 94,938.00 | 130.03 |
| ATF6A | 3 | 672.00 | 50,835.00 | 75.65 |
| CREB5 | 3 | 35.32 | 44,854.66 | 1270.06 |

C

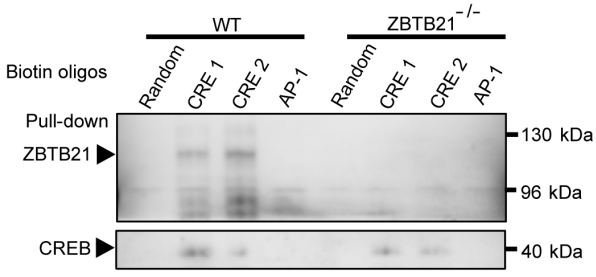


D

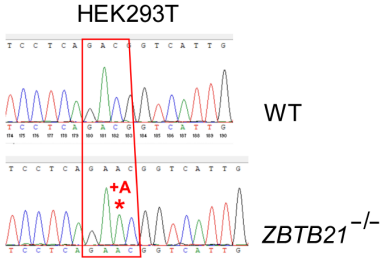


E

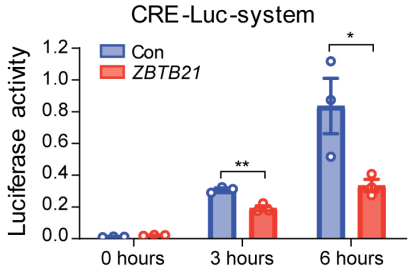


F

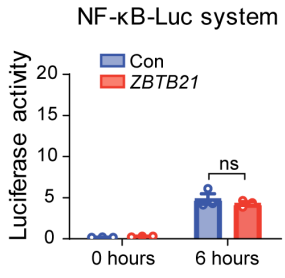


G

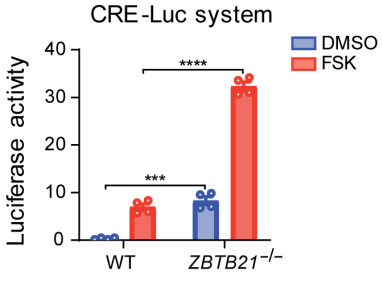


H

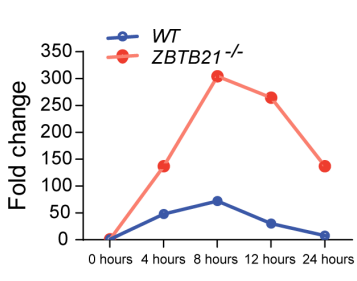


I

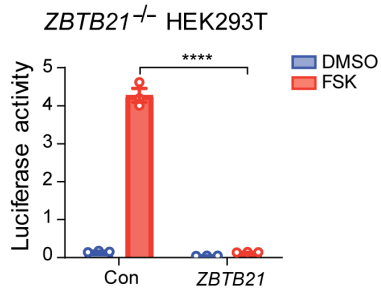


**Fig. 1. Identification of ZBTB21 as a suppressor of CRE-dependent gene transcription.** (**A**) Workflow diagram showing CRE-binding protein isolation using a biotin-labeled CRE DNA element and analysis by quantitative MS. (**B**) HEK293T cells transfected with biotin-CRE DNA element and treated with 10 μM forsklin (FSK) for 0, 30, and 60 min; proteins were pulled down, followed by MS analysis. (**C**) Pull-down assay using biotin-DNA element in WT and *ZBTB21*$^{-/-}$ HEK293T cells, analyzed by immunoblotting for ZBTB21 and CREB. (**D**) DNA sequence comparison of the *ZBTB21* locus in the WT and *ZBTB21*$^{-/-}$ HEK293T cells. (**E** and **F**) Effect of ZBTB21 overexpression on FSK-induced CRE (E) and TNFα-induced NF-κB (F) promoter activity. (**G** and **H**) Effect of ZBTB21 KO on FSK-induced CRE promoter activity at 6 hours (G) and various time points (H). (**I**) Rescue of ZBTB21 KO effect on FSK-induced CRE promoter activity by ZBTB21 reexpression. All data represent mean ± SEM. *P* values were determined by two-tailed Student's *t* tests. ns, not significant. **P* < 0.05, ***P* < 0.01, ***P < 0.001, and *****P* < 0.0001. Each sample in the experiments had three replicates, and independent experiments were performed at least two times. The data presented are representative results. DMSO, dimethyl sulfoxide.

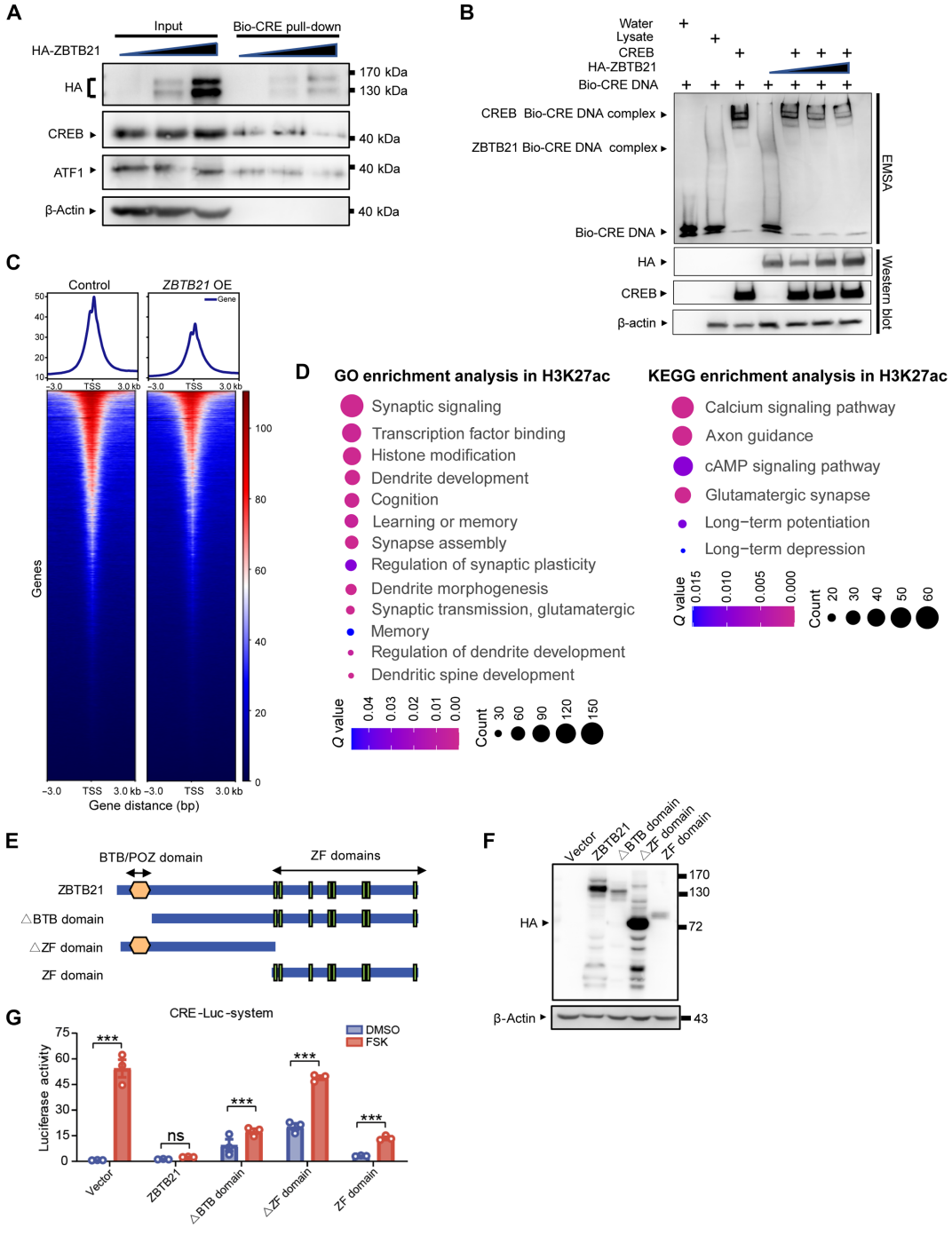


**Fig. 2. ZBTB21 competes with CREB for binding to the CRE and the domains essential for the suppression of CRE-dependent gene expression.** (**A**) HEK293T cells were transfected with HA-*ZBTB21* expression plasmid (0, 10, or 30 μg) and subsequently transfected with the biotin-CRE DNA element. The total cell lysates (input) and biotin-CRE pull-down were then analyzed by immunoblotting with antibodies as indicated. (**B**) Lysates of HEK293T cells overexpressing CREB and/or HA-*ZBTB21* as indicated were mixed with biotin-labeled CRE DNA. EMSA analysis of the binding between biotin-CRE and CREB in the presence of different amounts of ZBTB21 is shown. The proteins were analyzed by immunoblotting with antibodies as indicated. (**C**) Profile heatmap around the TSSs of H3K27ac-modified genes. Read counts were extracted for all CUT&Tag-seq experiments within a region spanning ±3 kb around the TSS. The blue-to-red gradient indicates high-to-low counts in the corresponding region ($P$ value < 0.05, $|\log_2\text{fold change}| > 1$), $n = 3$. (**D**) GO and Kyoto Encyclopedia of Genes and Genomes (KEGG) analyses of genes containing modified regions of H3K27ac. The top enriched biological process terms are displayed. The size of a circle indicates the number of enriched genes, and the color reflects the adjusted $P$ value ($|\log_2\text{fold change}| > 1$), $n = 3$. (**E** to **G**) Mapping ZBTB21 functional domains involved in transcriptional regulation. (E) Schematic depicting the generation of truncated *ZBTB21* expression constructs. (F) Immunoblot analysis of HA-tagged truncated ZBTB21 proteins. (G) HEK293T cells were cotransfected with plasmids expressing different domains of the ZBTB21 protein and the CRE-Luc reporter plasmid. Luciferase activity was measured after FSK stimulation. All data represent mean ± SEM. $P$ values were determined by two-tailed Student's $t$ tests. ***$P < 0.001$. Independent experiments were performed at least two times. The data presented are representative results.

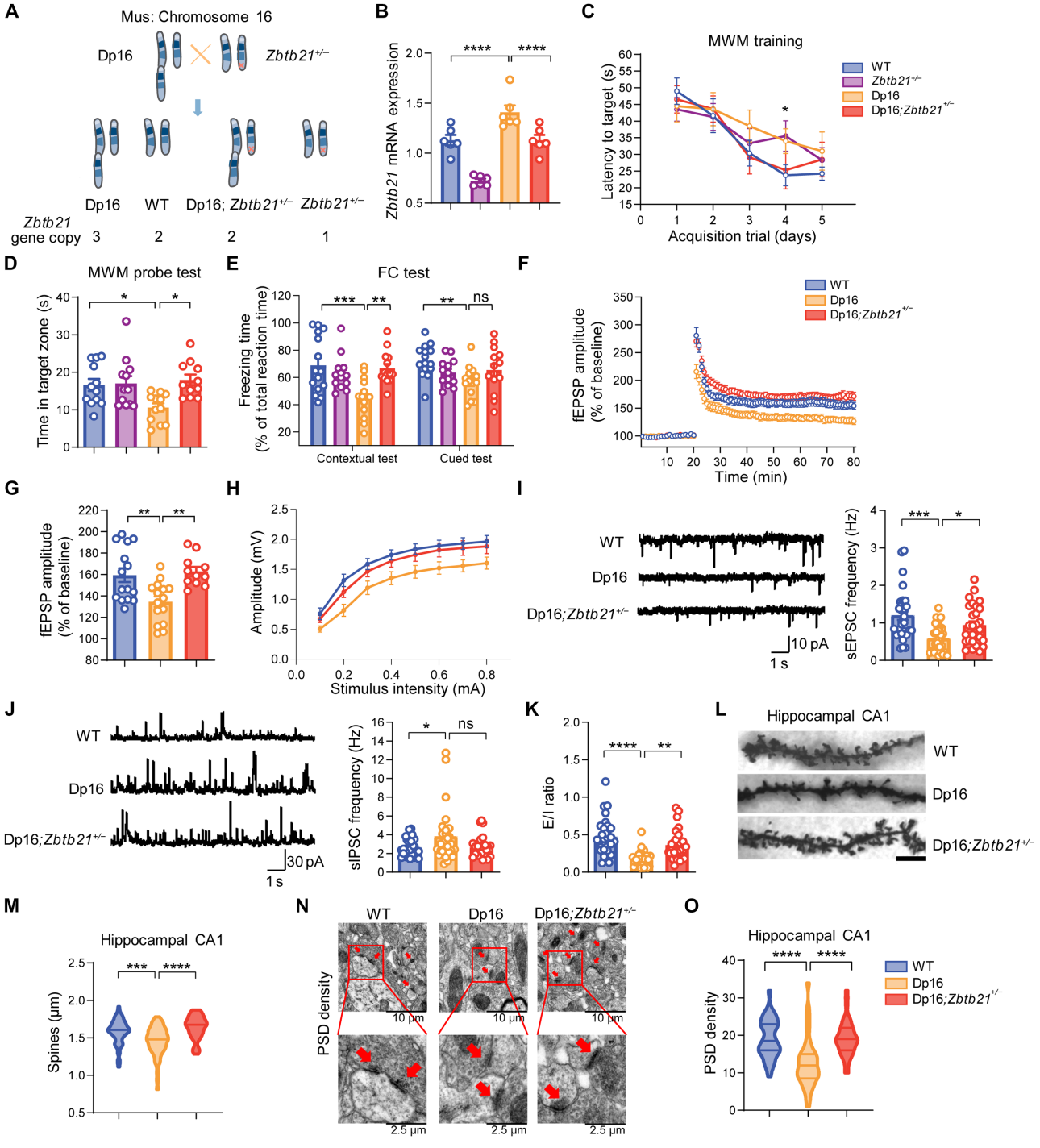


**Fig. 3. Normalizing the *Zbtb21* copy number restores synaptic and cognitive function in Dp16 mice.** (**A**) Mouse breeding strategy schematic. (**B**) Quantitative reverse transcription polymerase chain reaction (qRT-PCR) analysis of *Zbtb21* mRNA in hippocampi of 6-month-old WT, *Zbtb21*$^{+/-}$, Dp16, and Dp16;*Zbtb21*$^{+/-}$ mice ($n = 6$ each). (**C**) Time to target platform in MWM test for 6-month-old WT ($n = 12$ mice), *Zbtb21*$^{+/-}$ ($n = 12$ mice), Dp16 ($n = 12$ mice), and Dp16;*Zbtb21*$^{+/-}$ ($n = 11$ mice) mice. "*" on day 4: difference in time to reach platform, WT versus Dp16. (**D**) Time in the target quadrant during MWM probe test. (**E**) Percentage of freezing in fear conditioning tests. WT ($n = 15$ mice), *Zbtb21*$^{+/-}$ ($n = 13$ mice), Dp16 ($n = 14$ mice), and Dp16;*Zbtb21*$^{+/-}$ ($n = 14$ mice). (**F** and **G**) LTP recording in hippocampal CA1 region ($n = 6$ mice, 11 to 13 slices). (**H**) Input-output curve of basal synaptic transmission in hippocampal CA1 ($n = 6$ mice, 17 to 18 slices). (**I** and **J**) Spontaneous excitatory postsynaptic currents (sEPSC) and spontaneous inhibitory postsynaptic current (sIPSC) recordings in CA1 pyramidal neurons ($n = 27$ to 29 cells from four mice each). (**K**) Excitatory frequency/inhibitory frequency ratio in CA1 pyramidal neurons. (**L** and **M**) Golgi staining analysis of dendritic spine density in hippocampal CA1 ($n = 57$ to 62 dendrites from four mice each). Scale bar, 5 μm. (**N** and **O**) Electron microscopy analysis of synaptic structure and postsynaptic density (PSD) in hippocampal CA1 ($n = 36$ to 46 fields from three mice each). All data represent mean ± SEM. *P* values were determined by one-way analysis of variance (ANOVA) with Tukey's post hoc analysis. *$P < 0.05$, **$P < 0.01$, ***$P < 0.001$, and ****$P < 0.0001$.

M) and electron microscopy (Fig. 3, N and O, and fig. S2E). Our findings indicate that there are no significant differences in the lengths of embryos across the three genotypes, and morphologically, the embryos did not exhibit any significant disparities. Furthermore, we extended our investigation to assess the brain morphology of these mice. Our analysis revealed no notable differences in cortical thickness or the area of the hippocampus among Zbtb21$^{+/+}$, Zbtb21$^{+/-}$, and Zbtb21$^{-/-}$ mice. In addition, our experiments predominantly involved Zbtb21$^{+/-}$ breeding with Dp16 mice, including behavioral and electrophysiological analyses. Our results show no significant differences between the Zbtb21$^{+/-}$ mice and their WT littermates. This suggests that ZBTB21 haploinsufficiency has minimal impact on mouse behavior (fig. S2, F and G) and development (fig. S2, H and I) and demonstrated intact synaptic function (fig. S2, B to D). Together, these results suggest that ZBTB21 overdosage compromises synaptic function in the context of DS.

## Neuron-specific ZBTB21 overexpression results in synaptic and cognitive deficits

We further investigated the expression of ZBTB21 in various brain tissue cells of Dp16 mice. Compared to WT mice, ZBTB21 expression was higher in the Dp16 mice across these cell types. Notably, neurons exhibiting trisomy displayed the most pronounced increase in transcriptional levels (fig. S3, A to D). Furthermore, we analyzed ZBTB21 expression in the brains of individuals with DS, using data from a previously published study (*34*). The findings revealed that ZBTB21 expression in the brain tissue of DS individuals was markedly elevated in excitatory neurons when compared to the control group (fig. S3E). We further investigated the expression of *Zbtb21* in different cell types in the brain of WT mouse, finding it to be abundantly expressed in neurons and astrocytes (fig.S3F). To determine whether ZBTB21 overexpression in the nervous system leads to DS-like neuropathology, we generated Nestin-Cre;*Zbtb21*$^{LSL\text{-}Tg}$ conditional transgenic mice (Nestin-*Zbtb21*) by breeding Nestin-Cre mice with mice carrying the ROSA26-LSL-*Zbtb21* allele (*Zbtb21*$^{LSL\text{-}Tg}$) (Fig. 4A), and quantitative reverse transcription polymerase chain reaction (qRT-PCR) confirmed the increased expression of ZBTB21 in the hippocampus and in diverse cell types derived from Nestin-*Zbtb21* transgenic mice (fig. S4, A and B). We examined mouse cognitive performance and found that, compared with Nestin-Cre mice, Nestin-*Zbtb21* transgenic mice displayed impaired hippocampus-dependent learning and memory in the Morris water maze (MWM), novel object recognition (NOR), and fear conditioning (FC) tests (Fig. 4, B to D, and fig. S4C). Moreover, defects in hippocampal LTP (Fig. 4, E and F) and basal synaptic transmission (Fig. 4G) were also observed in Nestin-*Zbtb21* mice.

Furthermore, we performed Golgi staining and found a marked reduction in spine density in the hippocampus of Nestin-*Zbtb21* mice compared to Nestin-Cre mice (Fig. 4, H and I). Similar results were also observed in electron microscopy analysis (Fig. 4, J and K). Given that Nestin-Cre expresses Cre within neural progenitors and affects multiple cell types in the central nervous system (CNS) (*35*, *36*), to further characterize the contribution of neurons and astrocytes to ZBTB21-induced synaptic deficits, we generated Camk2a-Cre;*Zbtb21*$^{LSL\text{-}Tg}$ (Camk2a-*Zbtb21*) and Aldh1l1-ert2-Cre;*Zbtb21*$^{LSL\text{-}Tg}$ (Aldh1l1-ert2-*Zbtb21*) transgenic mice.

We first performed behavioral tests and found that neuron-specific overexpression of ZBTB21 markedly impaired cognitive performance in Camk2a-*Zbtb21* mice. These mice displayed significant deficits in hippocampus-dependent learning and memory in the MWM and FC tests. However, the impairment was not significant in the NOR test. This suggests that the cognitive deficits in Nestin-*Zbtb21* mice, which were more severe, might be due to a broader expression pattern of ZBTB21 (Fig. 5, A to C, and fig. S4, D to F). Consistent with the changes in behavioral performance, both synaptic function and density were compromised in the hippocampus of Camk2a-*Zbtb21* mice (Fig. 5, D to H). The Aldh1l1-ert2-*Zbtb21* mice demonstrated trends toward changes, but these were not statistically significant in the MWM test (fig. S5, A to E) and LTP recording (figs. S5, F to H). Together, these results suggest that neurons represent the major cell type affected by ZBTB21 overexpression in the DS brain.

## ZBTB21 binds to CREs in the promoter regions of genes in neurons

To elucidate the mechanism by which ZBTB21 contributes to synaptic and cognitive impairments, we infected mouse primary neurons with lenti-*Zbtb21* and analyzed the genome-wide DNA binding profile of *Zbtb21* using CUT&Tag-seq (fig. S1H).

We identified approximately 4700 potential ZBTB21 target sites in the promoter region (defined as ±3 kb from the TSS), using a significance threshold of $P$ value < 0.05 and $|\log_2\text{fold change}| > 1$. Notably, among the top consensus ZBTB21-binding motifs, three were CRE motifs (Fig. 6A). The analysis further revealed that the most significant enrichment of ZBTB21 binding occurred within promoter regions, introns, and distal intergenic regions (Fig. 6B). Specifically, the genes *Dcdc2a* and *Impact*, which are known to be involved in learning and memory (*37*–*39*), were used as examples to demonstrate the highly abundant ZBTB21 binding to the CRE motif in their promoters. Furthermore, CUT&Tag-seq revealed an enrichment of CRE binding (Fig. 6C). Similarly, chromatin immunoprecipitation (ChIP) analysis using an anti–hemagglutinin (HA) antibody in HA-*Zbtb21*–overexpressing mouse primary neurons detected a high level of ZBTB21 binding to the CRE in the promoter of *Crtcl (40*, *41*), another learning and memory-related gene (Fig. 6D). Together, our data indicate that ZBTB21 suppresses CRE-mediated transcription through direct binding with the canonical CRE in the promoter region of target genes.

## Restoration of ZBTB21 expression rescues synaptic function by correcting transcriptional defects in Dp16 mouse neurons

To gain further insight into the roles of ZBTB21 in DS pathogenesis by regulating CRE-mediated transcription, we performed whole-genome RNA sequencing (RNA-seq) on primary neurons from DS mice (WT, Dp16, and Dp16; *Zbtb21*$^{+/-}$). Our findings revealed that 420 genes, which were down-regulated in Dp16 mouse neurons [differentially expressed genes (DEGs) with a fold change > 1.2 and a $P$ value < 0.05], showed restored expression levels in Dp16;*Zbtb21*$^{+/-}$ neurons (Fig. 7A). GO enrichment analysis of these genes revealed their involvement in pathways related to cAMP-mediated signaling, learning and memory, and synaptic function (Fig. 7B). Notably, two-thirds of these 420 DEGs contained CRE motifs (Fig. 7C). Within these, 278 CRE-containing genes could be further categorized into four functional groups (Fig. 7D), with learning/memory and synapse-related pathways being significant categories. This suggests that CRE-containing genes are potential targets of ZBTB21 regulation, with a third of the non-CRE DEGs possibly indirectly regulated by ZBTB21. We

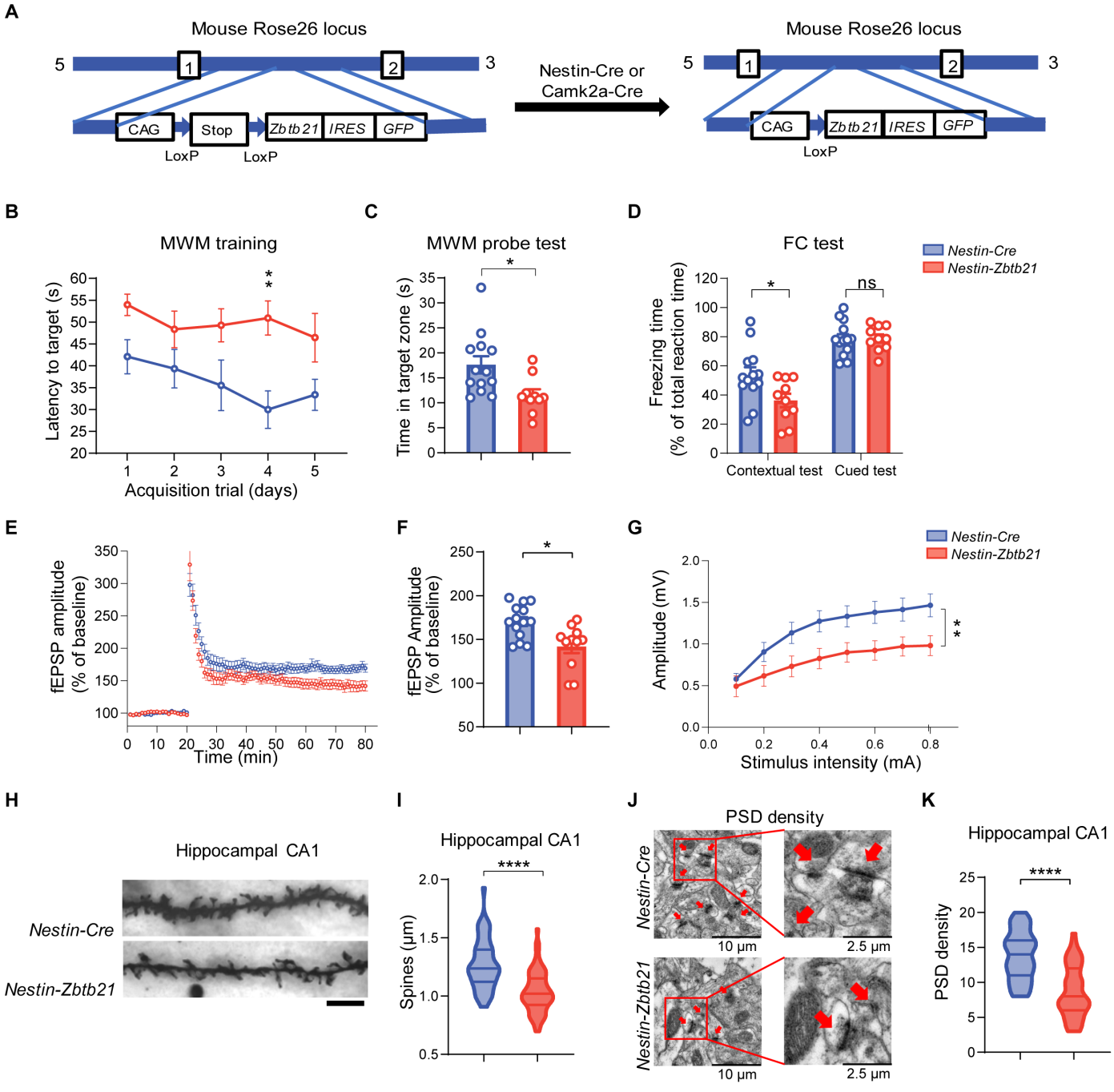


**Fig. 4. ZBTB21 overexpression in Nestin-*Zbtb1* transgenic mice phenocopies synaptic and cognitive deficits in DS mice.** (**A**) Generation of conditional *Zbtb21* transgenic mice by crossing CAG-Loxp-Stop-Loxp-*Zbtb21* (CAG-*Zbtb21*) mice with Nestin-Cre or Camk2a-Cre mice. (**B**) Time taken to reach the submerged target platform during the training phase of MWM test. (**C**) Time spent in the target quadrant during MWM probe test. (**D**) Percentage of freezing time in fear conditioning tests. Four-month-old Nestin-Cre mice ($n = 13$ mice) and Nestin-*Zbtb21* mice ($n = 10$ mice) were used in behavioral tests. (**E**) LTP recordings from the hippocampal CA1 region of 4-month-old Nestin-Cre ($n = 6$ mice, 14 slices) and Nestin-*Zbtb21* mice ($n = 6$ mice, 11 slices). (**F**) fEPSP amplitude of the last 10 min of LTP recording in (E). (**G**) Input-output curve of basal synaptic transmission in the hippocampal CA1 region of 4-month-old Nestin-Cre ($n = 6$ mice, 13 slices) and Nestin-*Zbtb21* mice ($n = 6$ mice, 11 slices). (**H** and **I**) Golgi staining analysis of dendritic spine density in the hippocampal CA1 region of mice. Representative images (H) and quantification (I) of dendritic spines in 4-month-old Nestin-Cre and Nestin-*Zbtb21* mice. Scale bar, 5 μm. $n = 4$ mice. (**J** and **K**) Electron microscopy analysis of synaptic structure and PSD in hippocampal CA1 region. $n = 60$ fields of view from three mice per group were counted. All data represent mean ± SEM. *P* values were determined by two-tailed Student's *t* tests. $^{*}P < 0.05$, $^{**}P < 0.01$, and $^{****}P < 0.0001$.

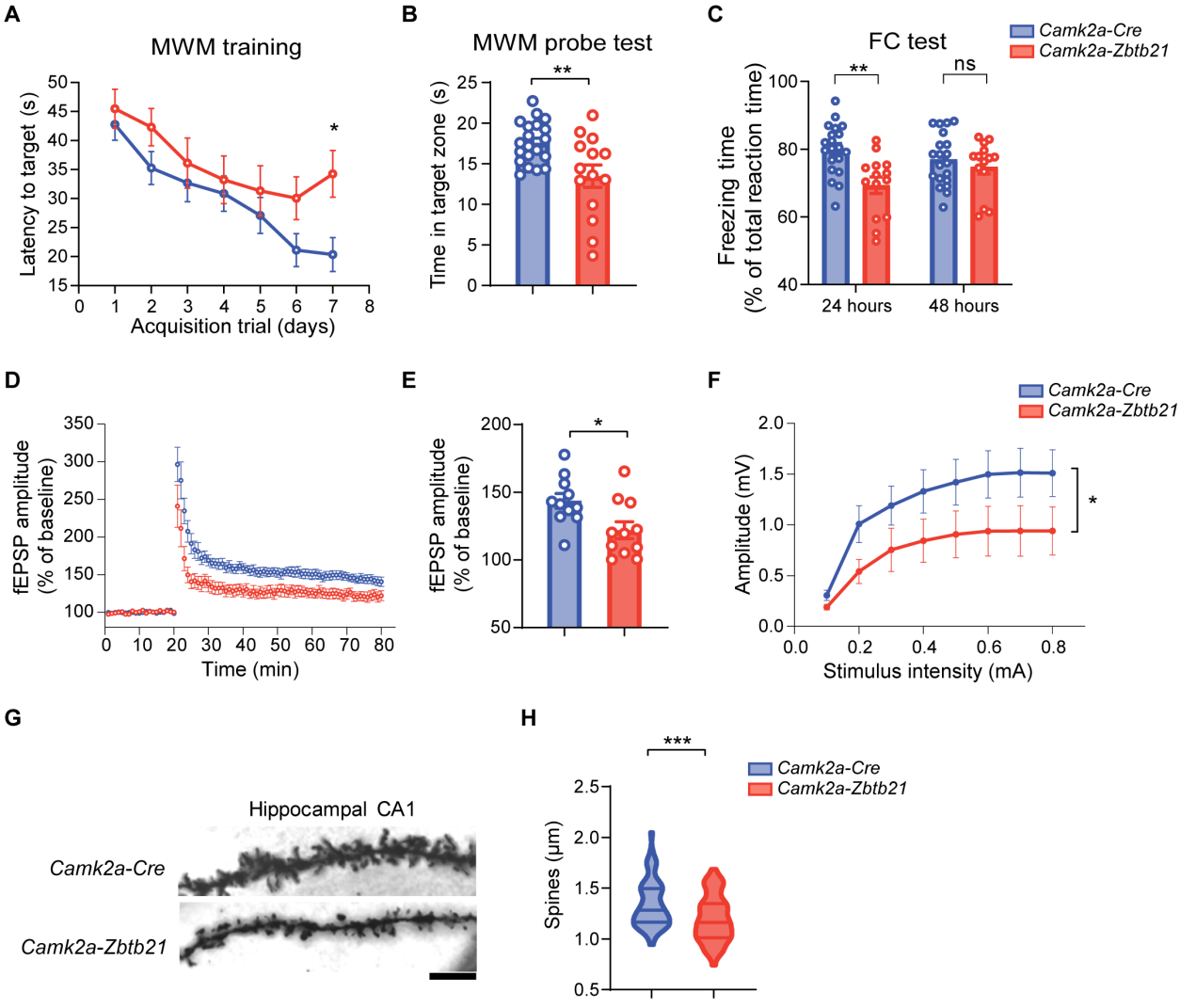


**Fig. 5. Neuronal ZBTB21 overexpression compromises synaptic and cognitive function in Camk2a-*Zbtb21* transgenic mice.** (**A**) Time taken to reach the submerged target platform during the training phase of the MWM test. (**B**) Time spent in the target quadrant in the MWM probe test; 4-month-old Camk2a-Cre ($n = 20$ mice) and Camk2a-*Zbtb21* mice ($n = 14$ mice) were used. (**C**) Percentage of freezing time in the fear conditioning tests. Four-month-old Camk2a-Cre ($n = 20$ mice) and Camk2a-*Zbtb21* mice ($n = 14$ mice) were used. (**D**) LTP recordings from the hippocampal CA1 region of 4-month-old Camk2a-Cre ($n = 6$ mice, 11 slices) and Camk2a-*Zbtb21* mice ($n = 6$ mice, 11 slices). (**E**) fEPSP amplitude of the last 10 min of LTP recording in (D). (**F**) Input-output curve reflecting basal synaptic transmission in the hippocampal CA1 region of 4-month-old Camk2a-Cre ($n = 6$ mice, 13 slices) and Camk2a-*Zbtb21* mice ($n = 6$ mice, 12 slices). (**G** and **H**) Golgi staining (G) and quantification (H) of dendritic spines in the hippocampal CA1 region of 4-month-old Camk2a-Cre and Camk2a-*Zbtb21* mice. Scale bar, 5 μm. $n = 4$ mice. All data represent mean ± SEM. *P* values were determined by two-tailed Student's *t* tests. $^*P < 0.05$, $^{**}P < 0.01$, and $^{***}P < 0.001$.

further reanalyzed the data from a previous study (*34*) to investigate the competitive relationship between ZBTB21 and CREB by examining the correlation between the expression levels of specific CRE motif–containing genes and *ZBTB21* in human DS brain tissues. Our analysis revealed a negative correlation between the expression of protocadherin 9, calcium dependent secretion activator 2, astrotactin 2 (which are important for synaptic function and cognition) and ZBTB21 expression (fig. S6A). These findings support the mechanism by which ZBTB21 competitively suppresses CREB-mediated transcription. A heatmap of the CRE-containing DEGs categorized as synapse-related genes is presented in Fig. 7E.

We further investigated the overlap between DEGs from CUT&Tag-seq and RNA-seq (Fig. 7F and fig. S6, B and C). We found 122 genes that were common to both datasets, 79 of which contained CRE motifs. GO enrichment analysis revealed that these overlapping genes were involved in pathways related to cAMP-mediated signaling, learning and memory, and synaptic function (Fig. 7G).

Together, these results demonstrate that the restoration of neuronal ZBTB21 expression to normal levels in Dp16 mice rescues synaptic and cognitive function in this model of DS, at least in part by restoring CRE-dependent transcription. The concordant restoration of CRE-dependent transcription provides evidence

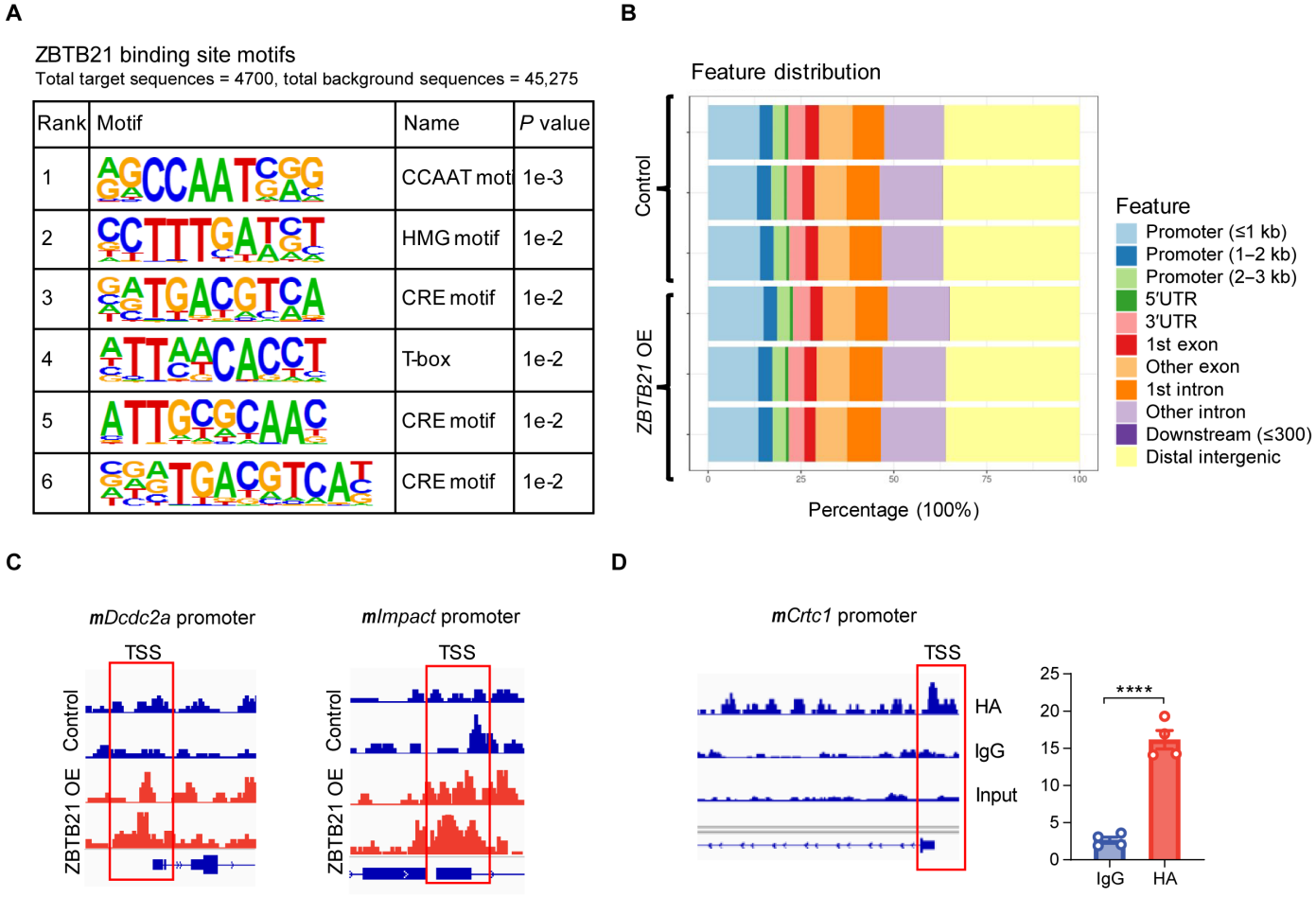


**Fig. 6. ZBTB21-induced inhibition of CRE-dependent gene expression is conferred by its binding to the CRE element.** (**A**) Homer software for different peak motif analyses (*P* value < 0.05, |$\log_2$fold change| > 1). The top six enriched motifs are shown. (**B**) Peak distributions relative to gene features. The majority of the peaks fell into promoters and intergenic regions. (**C**) Primary mouse neurons were infected with lenti-*HA-Zbtb21*, followed by chromatin CUT&TAG-seq analysis using an anti-HA antibody. The sequencing results were used to quantify the abundance of the CRE motif enriched by HA-ZBTB21. The distribution of ZBTB21 binding at the promoter region of *Dcdc2a* and *Impact* are shown. Red boxes indicate the regions that are enriched for ZBTB21 binding. (**D**) Primary mouse neurons were infected with lenti-*HA-Zbtb21*, followed by ChIP analysis using an anti-HA antibody. The sequencing results were used to quantify the abundance of the CRE motif enriched by HA-ZBTB1. The distribution of ZBTB21 binding at the promoter region of *Crtc1* is shown. The red box indicates the region that shows enrichment for ZBTB21 binding. Enrichment of ZBTB21 binding in the promoter region of *Crtc1* in the box was confirmed by qPCR and is shown in the right. All data represent mean ± SEM. *P* values were determined by two-tailed Student's *t* tests. ****$P < 0.0001$. 5′UTR, 5′ untranslated region; IgG, immunoglobulin G.

that reducing ZBTB21 acts through this mechanism to ameliorate DS-related phenotypes.

## DISCUSSION

While the CREB family of proteins is well-recognized for its pivotal role in regulating synaptic function, learning and memory, the pathological implications and regulatory mechanism of CRE-dependent gene expression remain largely unexplored. This study uncovers that overdosage of the chromosome 21–encoded gene *ZBTB21* contributes to the dysregulation of CRE-dependent gene expression and synaptic dysfunction in the DS brain. Our findings suggest that the detrimental impact of ZBTB21 overdosage on CRE-dependent gene expression in the DS brain is a key contributing factor to synaptic and cognitive deficits (fig. S7). This finding is further supported by a previous study that demonstrated a close link between human segmental trisomy containing the *ZBTB21* locus and intelligence quotient levels in individuals with DS (*42*).

Previous research has reported impaired cAMP production in the hippocampus of a murine DS model (*26*). Rolipram, a phosphodiesterase inhibitor, has been shown to ameliorate behavioral abnormalities in mice with cognitive impairment by elevating neuronal cAMP levels (*43*–*45*). In addition, gonadotropin-releasing hormone (GnRH) therapy, which enhances cAMP levels, has demonstrated beneficial effects in individuals with DS and DS model mice (*46*–*48*). Overcoming the impairment of the cAMP-CREB pathway could potentially benefit individuals with DS. Given that *ZBTB21* overdosage suppresses CRE-dependent gene expression, increasing cAMP levels may be a potential approach to compensate for the inhibition of CRE-dependent gene expression induced by trisomy 21. *RCAN1*, a DSCR gene that plays a crucial role in learning and memory, is known to be negatively regulated by proteasomal degradation in a

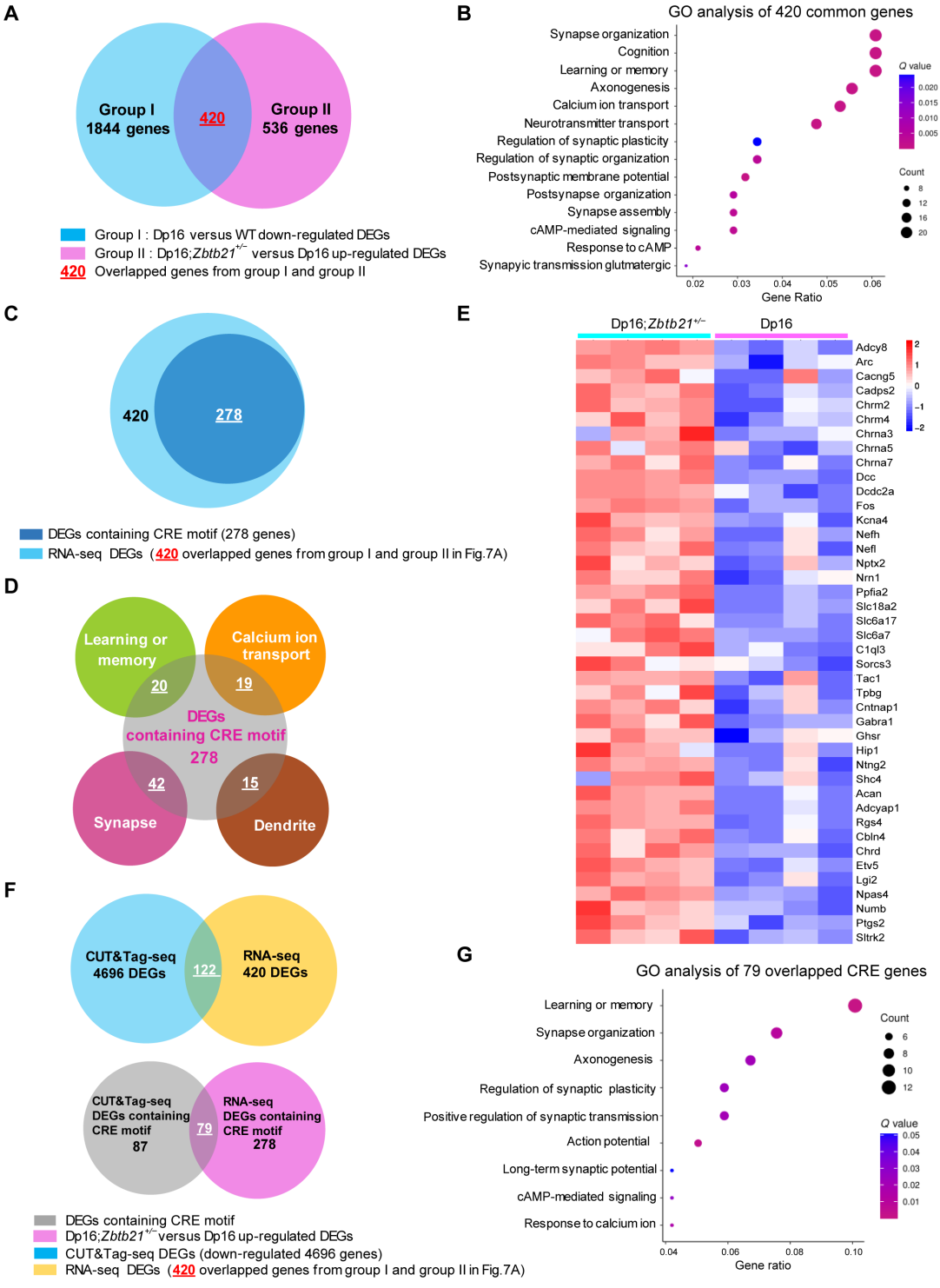


**Fig. 7. Normalizing the *Zbtb21* copy number rescues synaptic function by correcting transcriptional defects in Dp16 mouse neurons.** (**A**) Venn diagram depicting up-regulated genes in Dp16;*Zbtb21*$^{+/-}$ mice relative to Dp16 mice and down-regulated genes in Dp16 mice relative to WT mice. The 420 genes in the overlapping region indicate down-regulated genes in Dp16 restored by *Zbtb21* normalization. (**B**) GO analysis of the overlapping genes in (A). The top enriched biological process terms are displayed. The size of a circle indicates the number of enriched genes, and the color reflects the adjusted *P* value. (**C**) The outside circle represents the 420 overlapping genes in (A), and the inside circle shows the 278 genes containing CRE motifs among these 420 DEGs. (**D**) The central circle represents the 278 CRE-containing DEGs in (C), and the petals show the number of CRE-containing DEGs classified into different categories. (**E**) Heatmap depicting the 42 synapse-related genes identified in (D). (**F**) Venn diagram depicting the overlapping CRE motif–containing genes from RNA-seq and CUT&TAG-seq. (**G**) GO analysis of the overlapping CRE-containing genes in (F). The top enriched biological process terms are displayed. GO enrichment analysis was performed under the filtering condition of a *q* value of 0.05.

CREB transcriptional activation-dependent manner (*49*,*50*). The suppression of CRE-dependent gene expression by ZBTB21 could form a feedforward loop with RCAN1, exacerbating DS-associated cognitive deficits.

The ZBTB21 protein is expressed in multiple cell types within the CNS. While we have demonstrated that neuronal ZBTB21 is important for learning and memory, its roles in other cell types remain to be further characterized. We observed that the defects in Nestin-*Zbtb21* mice were more severe than those in Camk2a-*Zbtb21* mice, suggesting that multiple cell types in the CNS may contribute to neurological phenotypes in *Zbtb21* transgenic mice. Moreover, Nestin-Cre–mediated targeting of progenitor cells could result in ZBTB21 overexpression at the embryonic stage, which might also explain the stronger phenotype observed in Nestin-*Zbtb21* mice. Future studies analyzing the effects of conditional *Zbtb21* deletion in various CNS cell types will be necessary to characterize the cell type–specific effects of ZBTB21 perturbation in the CNS.

The potential benefits of rolipram or GnRH treatment support the restoration of cAMP levels as a possible strategy to treat DS-related cognitive deficits. Considering the critical role of ZBTB21 in suppressing CRE-dependent gene expression, further investigation into the function of ZBTB21 may provide insights into therapeutic strategies aimed at preventing or treating DS-related cognitive deficits by restoring CRE-dependent gene expression.

## MATERIALS AND METHODS

### Experimental animals

Dp16 mice (stock no. 013530), Nestin-Cre mice (stock no. 003771), and Camk2a-Cre mice (stock no. 005359) were obtained from the Jackson Laboratory (Bar Harbor, Maine, USA). Aldh1l1-ert2-Cre mice were generated as described previously by Hu *et al.* (*51*). Zbtb21$^{-/-}$ mice were obtained from genetically modified fertilized eggs by injecting two strips of single guide RNA targeting the largest exon region of Zbtb21 and Cas9 mRNA into fertilized mouse eggs. Rosa26-*Zbtb21* mice were generated using CRISPR-CAS9 technology. A plasmid (Rosa26-CAG-floxp-stop-floxp-*Zbtb21*) containing the *Zbtb21* gene and its regulatory elements was integrated into the mouse Rosa26 locus through homologous recombination. This plasmid uses the LoxP-Stop-LoxP (LSL) cassette, which enables conditional activation of gene expression in mammalian cells and animals through Cre-mediated recombination. After Cre-mediated recombination, the LSL cassette was excised, allowing for the transcription and expression of the gene of interest.Camk2a-*Zbtb21* mice were generated by crossing Rosa26-*Zbtb21* mice with Camk2a-Cre mice, resulting in neuron-specific overexpression of ZBTB21 driven by a ubiquitous CAG promoter. A stop codon cassette was flanked by two LoxP sites. The STOP codon was expressed before Cre-mediated recombination. After Cre-mediated recombination, the STOP codon cassette was excised, and the *Zbtb21* gene was expressed instead of the STOP codon.Nestin-*Zbtb21* mice were generated by breeding Rosa26-*Zbtb21* mice with Nestin-Cre mice, resulting in the overexpression of ZBTB21 specifically in CNS precursor cells. The breeding strategy used for the generation of Nestin-*Zbtb21* mice was the same as that used for Camk2a-*Zbtb21* mice.Aldh1l1-ert2-*Zbtb21* mice were generated by crossing Rosa26-*Zbtb21* mice with Aldh1l1-ert2-Cre mice, resulting in astrocyte-specific overexpression of ZBTB21. The breeding strategy used for the generation of the Aldh1l1-ert2-*Zbtb21* mice was identical to that used for the Camk2a-*Zbtb21* mice.

All the experimental mice used in our study were bred and maintained on a C57BL/6J background. Specifically, only male mice were used for the animal experiments mentioned in our work, which were performed according to the guidelines of the Institutional Animal Care and Use Committee of Xiamen University. The primers used for genotyping are shown in table S1.

### Cell culture

Primary neurons were grown and maintained in neurobasal medium (Thermo Fisher Scientific, 21103-049) supplemented with B27 (Thermo Fisher Scientific, 17504044) and 1% penicillin/streptomycin. For primary astrocyte cultures, both hemicortices of mice on postnatal days 1 to 2 were dissected and chopped into small pieces. The tissue was dispersed by pipetting. After centrifugation, the cell pellet was resuspended in Dulbecco's modified Eagle's medium (DMEM)/F12 culture medium (Thermo Fisher Scientific, 10565-018) containing 10% fetal bovine serum (FBS) and 1% penicillin/streptomycin. The cells were seeded in culture flasks, and the culture medium was changed by half every 3 days. After 7 days, the mixed culture was mechanically agitated at 180 rpm for 1 hour. The astrocytes were then dissociated using trypsin-EDTA and plated in 60-mm plates for RNA extraction. HEK293T cells were cultured in DMEM (Gibco, C11995500BT) supplemented with 10% FBS and 1% penicillin/streptomycin. For primary microglial cultures, both hemicortices of mice on postnatal days 1 to 2 were dissected and chopped into small pieces. The tissue was dispersed by pipetting. After centrifugation, the cell pellet was resuspended in DMEM culture medium (Gibco, C11995500BT) containing 10% FBS and 1% penicillin/streptomycin. The cells were then seeded in culture flasks. Granulocyte-macrophage colony-stimulating factor (25 ng ml$^{-1}$; R&D Systems, Minneapolis, MN, USA; 415-ML-050) was added to the cultures after 3 days. Primary microglia were harvested by shaking the flasks at 180 rpm for 1 hour, 10 to 12 days after plating, and once every 3 days thereafter for RNA extraction.

### Drug administration

Tamoxifen (MedChemExpress, HY-13757A) was used to induce Cre$^{ERT2}$-mediated recombination. Tamoxifen was dissolved in 90% corn oil (Sigma-Aldrich, C8267). Adult P56-60 mice were subjected to daily intraperitoneal injections of tamoxifen (80 mg/kg) for seven consecutive days, as previously described (*52*). 4-Hydroxy tamoxifen (Sigma-Aldrich, H7904-5MG) was used to induce CreERT2-mediated recombination in primary cell, the final concentration of 4-hydroxy tamoxifen is 5 μM, and incubated for 6 days.

### Fear conditioning test

The experimental mice were placed in a conditioning chamber (Noldus, Ugo Basile) and allowed to freely explore for a period of 2 min. Following the exploration phase, a 30-s voice prompt was presented as the conditioned stimulus (CS). During the last 2 s of the voice prompt, the mice received 0.8-mA foot electrical stimulation as an unconditioned stimulus (US). The voice prompt accompanied by the electric stimulus (CS-US) was repeated every minute for the subsequent 3 min. For the contextual test, the mice were reintroduced to the same chamber 24 hours later and allowed to explore the familiar environment for 5 min without any stimulation. For the cued test, the mice were placed in a new test room with a different contextual environment for 2 min, followed by 3 min of voice prompts.

### NOR test

The NOR test was conducted as previously described (*52*). On day 1, each mouse was acclimated to the test chamber for 5 min. On day 2, two objects of identical shape and size were positioned diagonally within the home cage. Subsequently, the mice were placed in the center of the cage and allowed to freely explore the open field environment and objects for 10 min to become familiar with them. On day 3, one of the objects remained unchanged, while the other object was replaced with a block that closely resembled a different shape. The mice were then placed in the center of the cage again and allowed to explore freely for 10 min. The time spent by the mice investigating the old object and the new object was recorded.

### MWM test

The experiment was conducted in a quiet indoor circular pool with a diameter of 120 cm, maintaining a constant water temperature of 22° ± 1°C. A fixed platform (10 cm in diameter) was placed in a preset target quadrant and submerged approximately 1 cm beneath the water surface. The pool was adorned with black geometric symbols on the diagonal walls, which served as cues for the mice to find the platform. During the training phase, the mice were released from one of six randomized positions, and two trials were performed every day for four to five consecutive days. Each mouse was given 60 s to find the hidden platform, and if a mouse failed to find the platform within 60 s, then it was guided to the platform by the experimenter and left there for 30 s. During the test phase, the platform was removed, and the mice were placed in the water from the predetermined test point. The time taken by the mice to reach the platform and the percentage of time spent in the quadrants were recorded using a Noldus EthoVision system.

### Preparation of mouse brain sections

After anesthesia, the mouse brain was removed and then kept in precooled oxygen-saturated (95% $O_2$ and 5% $CO_2$) high-glucose buffer [64 mM NaCl, 2.5 mM KCl, 1.25 mM $NaH_2PO_4$, 10 mM $MgSO_4$, 26 mM $NaHCO_3$, 10 mM D-glucose, 120 mM sucrose, and 0.5 mM $CaCl_2$ (pH 7.4); osmotic pressure, 290 to 320 milliosmol (mOsm)]. The 400-μm-thick slices were obtained using a vibrator (VT1200S, Leica, Germany). Once the brain sections were acquired, the slices were promptly transferred to oxygen-saturated artificial cerebrospinal fluid [ACSF; 120 mM NaCl, 3.5 mM KCl, 1.25 mM $NaH_2PO_4$, 1.3 mM $MgSO_4$, 26 mM $NaHCO_3$, 10 mM D-glucose, and 2.5 mM $CaCl_2$ (pH 7.4); osmotic pressure, 290 to 320 mOsm] at a constant temperature of 32°C and incubated for 1 hour, followed by an additional 1-hour incubation at room temperature. For electrophysiological recording, the slices were transferred to a recording chamber, where they were continuously perfused with oxygen-saturated (95% $O_2$ and 5% $CO_2$) standard ACSF at 32°C.

### Electrophysiological recording

Electrophysiological recording was performed using a MultiClamp 700B amplifier (MD/Axon US). The acquired data were subsequently analyzed using pClamp software (version 10.6, Molecular Devices).

### Input-output recording

The field excitatory postsynaptic potential (fEPSP) was evoked by the stimulation electrode as mentioned. Once the amplitude of the fEPSP reached a stable level and remained consistent for a minimum of 10 min, a series of electrical stimulations was applied, gradually increasing in intensity. The intensities used were 100, 200, 300, 400, 500, 600, 700, and 800 μA. The amplitude of the fEPSP corresponding to each stimulus intensity was recorded. This collection of data resulted in an input-output (*I-O*) curve, reflecting the response capacity of the synapses under different stimulus intensities.

### LTP recording

Responses were elicited by electrically stimulating the Schaffer collateral pathway using a concentric electrode. fEPSPs were recorded in the hippocampal CA1 region using a patch-type pipette filled with ACSF (Re = 2 to 3 megohm). The baseline stimulus intensity was adjusted to evoke fEPSPs with amplitudes at approximately 30% of the maximum response obtained from the input-output function. The interval between each electrical stimulation was set to 20 s, and the electrode resistance ranged from 1 to 3 megohm. Stable baseline recordings were obtained for at least 20 min before the high-frequency stimulation (HFS) used to induce hippocampal LTP. The HFS consisted of two trains of stimuli delivered at 100 Hz, with an interval of 30 s. Following the HFS, a 60-min recording of the baseline protocol was performed.

### Golgi staining

Golgi staining was performed using an FD Rapid Golgi Stain Kit (FD Neuro Technologies) following the manufacturer's instructions. Subsequently, Z-stack images were acquired with a Leica SP8 confocal microscope, and the density of the dendritic spines was analyzed using National Institutes of Health ImageJ software.

### CUT&Tag assay

The CUT&Tag assay was performed using the Hyperactive Universal CUT&Tag Assay Kit for Illumina (Vazyme) according to the manufacturer's instructions. Briefly, the membranes of $2 \times 10^5$ primary neurons were permeabilized with concanavalin A–coated magnetic beads and a non-ionic detergent (digitonin). Subsequently, cells were incubated with primary antibodies, either H3K27ac (1:500; Cell Signaling Technology, catalog no. 8173) or anti-HA (1:100; Santa Cruz Biotechnology, sc-7392 X), at 4°C overnight. Through the binding of the primary antibody to the target protein, corresponding secondary antibody, and Protein A/G, Tn5 transposases fused with Protein A/G are precisely targeted to cut the DNA sequence near the target protein. During the DNA cleavage by the transposase, adapter sequences are added to both ends of the cut fragment, which can be directly amplified by PCR to form a library for high-throughput sequencing. Libraries were constructed using the TD202 TruePrep Index Kit V2 for Illumina (Vazyme). Sequencing was performed using Illumina NovaSeq 6000 system. Peak calling was performed using sparse enrichment analysis, and subsequent data analysis was conducted using HOMER, a software suite for CUT&TAG analysis.

### Quantitative MS

Biotin-conjugated double-stranded DNA was prepared and introduced into HEK293T cells as previously described (*53*). Subsequently, the cells were stimulated to facilitate the binding of transcription factors to the DNA. Streptavidin agarose was used to precipitate the DNA. The binding proteins were denatured from the eluted DNA using SDS. The denatured proteins were then processed and subjected to MS analysis on a TripleTOF 5600 (Sciex) mass

spectrometer coupled to a NanoLC Ultra 2D Plus (Eksigent) high-performance liquid chromatography system.

### RNA isolation and quantitative reverse transcription PCR

Total RNA was extracted using the RNAiso Plus reagent (TaKaRa, Japan; D9109), and 3 μg of total RNA was reverse-transcribed into cDNA using M-MLV Reverse Transcriptase (RNase $H^+$) (The Beijing Genomics Institute, China; EM-004). Real-time PCR was performed on a LightCycler 480 System (Roche, Mannheim, Germany) using ChamQ Universal SYBR qPCR Master Mix (Vazyme, China; Q711-02). Data analysis was performed using the $2^{-\triangle\triangle Ct}$ method after normalization to the *ActB* internal control. The primers used in RT-PCR are shown in table S1.

### RNA sequencing

RNA-seq was performed using the Illumina NovaSeq 6000 system. The raw RNA-seq reads were aligned to the Ensembl mouse reference genome GRCm39. The raw gene counts were processed using the DESeq2 package (version 1.20.0) clusterProfiler (version 3.8.1, pvalueCutoff = 0.05). GO enrichment analysis of DEGs was performed in R using the package clusterProfiler (version 3.8.1, qvalueCutoff = 0.05).

### DNA pull-down assays

#### *Intracellular assay*

Biotin-labeled double-stranded DNA (Random: CAGGTATC; CRE1: TGACGTCA; CRE2: ATGACGTA; AP-1: TGACTCA) was transfected into HEK293T cells. After 24 hours, the cells were lysed in lysis buffer [recipe of lysis buffer can be found in (*54*)]. The lysates were incubated on ice for 30 min and then centrifuged at 20,000*g* for 30 min at 4°C. The supernatant was precipitated with NeutrAvidin Agarose Resins (Thermo Fisher Scientific) at 4°C for 30 min. The resins were then washed four times with lysis buffer, and the DNA binding proteins were denatured and eluted using 2% SDS. The eluted proteins were prepared using a standard protocol for MS or Western blot analysis.

#### *Extracellular assay*

The ZBTB21 overexpression plasmid was transfected into HEK293T cells. After 24 to 36 hours, the HEK293T cells were lysed in lysis buffer. The lysates were incubated on ice for 30 min and then centrifuged at 20,000*g* for 30 min at 4°C. Biotin-conjugated double-stranded DNA was added to the supernatant and rotated for 2 hours. NeutrAvidin Agarose Resins (Thermo Fisher Scientific) were then added to the supernatant and rotated for 30 min. The resins were washed four times with lysis buffer, and the DNA binding proteins were denatured and eluted using 2× sample buffer. The eluted proteins were prepared using a standard protocol for Western blot analysis.

### *ZBTB21* KO cell line

The targeting sequence in the guide RNA (gRNA) vector for human *ZBTB21* was 5′-catcgacaatgaccgtctg-3′. First, the gRNA with the Cas9 expression plasmid was cotransfected into WT HEK293T cells. The transfected cells were then incubated with blasticidin to facilitate selection. After selection, single-cell clones were isolated from the pool of transfected cells using a limiting dilution cloning technique in 96-well plates. Each well contained only a single cell to ensure clonality. The isolated clones were subsequently screened for the KO genotype by Sanger sequencing.

### Electrophoretic mobility shift assay

EMSAs were performed as previously described (*55*) using the LightShift Chemiluminescent EMSA Kit (Pierce, 20148). Briefly, protein extraction from overexpressed HEK293T cells was achieved using the repeated freeze-thaw method, followed by the standard EMSA protocol using the EMSA Kit.

### Chromatin immunoprecipitation

ChIP was conducted as previously described (*56*). Briefly, primary neurons infected with lentivirus were fixed for 10 min at room temperature with phosphate-buffered saline (PBS) containing 1% formaldehyde (Thermo Fisher Scientific, 28908), and the reaction was stopped by adding 125 mM glycine for 5 min. Subsequently, the cells were washed twice with ice-cold PBS. Fixed cells were then collected by centrifugation at 12,000 rpm for 30 s and resuspended in lysis buffer. DNA fragmentation was achieved by sonication using a Bioruptor Plus (Diagenode), resulting in sheared DNA fragments ranging from 150 to 500 base pairs. The sonicated cell lysate was diluted 10-fold in ChIP dilution buffer and incubated with HA antibody (Abcam, ab9110) and isotype immunoglobulin G (Sino Biological, CR1) for 4 to 8 hours at 4°C, followed by a 2-hour incubation with magnetic beads coated with protein G. After thorough washing and elution, the protein-DNA cross-linking complex was decrosslinked in TE (pH8.0 1M Tris-HCL; 0.5M EDTA)-SDS buffer by overnight heating at 65°C. Immunoprecipitated DNA was purified using DNA recovery columns (Qiagen, 28104) and subsequently analyzed by qPCR using CFX96 (Bio-Rad).

### Electron microscopy analysis

Tissue collection and transmission electron microscopy (TEM) were performed as previously described (*57*). Briefly, mice were deeply anesthetized and perfused with ice-cold PBS. The hippocampus was dissected and fixed with 2.5% glutaraldehyde at 4°C for 2.5 hours. Afterward, the tissue was washed three times with PBS. Fixed tissue processing and TEM were performed according to the standard electron microscopy protocol.

### Lentiviral packaging

Lentiviral packaging was conducted as previously described (*58*). Briefly, HEK293T cells were transfected with expression vectors containing *Zbtb21* and lentiviral packing plasmids (PMDL/REV/VSVG) using the calcium phosphate precipitation method. After 8 to 12 hours, the cell culture medium was replaced, and the virus-containing medium was collected 36 hours later.

### cAMP concentration assay

The cAMP concentration assay was performed following the protocol described previously (*59*), using the cAMP-Glo Max Assay (V1681, Promega). The standard assay protocol was followed using the abovementioned cAMP levels assay kit.

### PKA activity assay

The PKA activity assay was performed using the PKA Colorimetric Activity Kit (EIAPKA, Invitrogen), following the standard assay protocol provided with the abovementioned reagent kit. Briefly, the 293T cells in a 60-mm dish were lysed using 1 ml of lysis buffer, and the lysate was then diluted 20-fold for activity testing.

### Immunoblot analysis

Immunoblot analysis was performed as previously described (*53*). Antibodies were used as follows: anti-ZBTB21 (1:500; Proteintech, 20132-1-AP), anti-CREB (1:1000; Abclonal, A11989), anti-HA (1:5000; Biochee, A2022-02L), anti-ACTIN (1:5000; Affinity, T0022), and anti-TUBULIN (1:5000; Abmart, M20005M).

### Nissl staining

Nissl staining was performed following the protocol as described previously (*52*). Briefly, frozen sections were stained with Nissl staining solution (Beyotime) for 10 min. The staining process was terminated with water, and the slides were decolorized using ethanol, followed by clearing with xylene for imaging observation.

### Imaging *Zbtb21* mRNA in brain tissue using hybridization chain reaction

The hybridization chain reaction technique was adapted from previous work by Pierce *et al.* (*60*), with minor modifications. Briefly, 15-μm-thick paraformaldehyde-fixed brain tissue cryosections were prepared. Following washes with PBS, the sections were incubated in 70% ethanol at −20°C overnight. This was followed by two washes with 2× SSC, and the sections were prehybridized with 30% probe hybridization buffer at 37°C for 30 min. Subsequently, hybridization was performed overnight at 37°C with a final concentration of 4 nM detection probe in 30% probe hybridization buffer. Afterward, the sections were washed with 30% probe wash buffer preheated to 37°C, followed by two washes with 5× SSC-Tween buffer. The sections were then preamplified for 30 min using amplification buffer. The fluorescent probe was annealed and diluted in amplification buffer to a final concentration of 40 nM, followed by overnight incubation. Last, the sections were stained with Hoechst to visualize the nuclei, rinsed once, and mounted for observation. The detection probes were designed to target 23 pairs of target sites specific to mouse *Zbtb21* mRNA. The B5 probe set was selected for amplification, and Alexa Fluor 568 fluorescence was used for labeling.

### Quantification and statistical analysis

GraphPad Prism 8.0 software was used to analyze the data. Statistical differences between the two groups were assessed using paired or unpaired *t* tests. Differences among multiple groups were assessed using one-way analysis of variance (ANOVA), followed by Bonferroni's post hoc analysis. The statistical significance of the differences between groups was determined in accordance with the following criteria: not significant, $P > 0.05$; $*P < 0.05$; $**P < 0.01$; $***P < 0.001$; and $****P < 0.0001$.

### Study approval

Animal experiments were reviewed, approved, and approved by the Laboratory Animal Management and Ethics Committee of Xiamen University (approval number XMULAC20210070) and were performed in strict accordance with good animal practices as defined by Xiamen University Laboratory Animal Center (Xiamen, China). The mice used in this study were housed under specific pathogen–free conditions with a 12-hour light/dark cycle and access to food and water ad libitum at the Xiamen University Laboratory Animal Center.

## Supplementary Materials

**This PDF file includes:**

Figs. S1 to S7
Table S1

## REFERENCES AND NOTES


1. Z. Li, T. Yu, M. Morishima, A. Pao, J. LaDuca, J. Conroy, N. Nowak, S. Matsui, I. Shiraishi, Y. E. Yu, Duplication of the entire 22.9 Mb human chromosome 21 syntenic region on mouse chromosome 16 causes cardiovascular and gastrointestinal abnormalities. *Hum. Mol. Genet.* **16**, 1359–1366 (2007).
2. C. Ferencz, C. A. Neill, J. A. Boughman, J. D. Rubin, J. I. Brenner, L. W. Perry, Congenital cardiovascular malformations associated with chromosome abnormalities: An epidemiologic study. *J. Pediatr.* **114**, 79–86 (1989).
3. S. E. Antonarakis, B. G. Skotko, M. S. Rafii, A. Strydom, S. E. Pape, D. W. Bianchi, S. L. Sherman, R. H. Reeves, Down syndrome. *Nat. Rev. Dis. Primers* **6**, 9 (2020).
4. K. Gardiner, A. C. Costa, The proteins of human chromosome 21. *Am. J. Med. Genet. C Semin. Med. Genet.* **142C**, 196–205 (2006).
5. L. E. Becker, D. L. Armstrong, F. Chan, Dendritic atrophy in children with Down's syndrome. *Ann. Neurol.* **20**, 520–526 (1986).
6. R. Weitzdoerfer, M. Dierssen, M. Fountoulakis, G. Lubec, Fetal life in Down syndrome starts with normal neuronal density but impaired dendritic spines and synaptosomal structure. *J. Neural Transm. Suppl.*, 59–70 (2001).
7. M. Suetsugu, P. Mehraein, Spine distribution along the apical dendrites of the pyramidal neurons in Down's syndrome. A quantitative Golgi study. *Acta Neuropathol.* **50**, 207–210 (1980).
8. B. S. Scott, L. E. Becker, T. L. Petit, Neurobiology of Down's syndrome. *Prog. Neurobiol.* **21**, 199–237 (1983).
9. T. L. Petit, J. C. LeBoutillier, D. P. Alfano, L. E. Becker, Synaptic development in the human fetus: A morphometric analysis of normal and Down's syndrome neocortex. *Exp. Neurol.* **83**, 13–23 (1984).
10. B. Schmidt-Sidor, K. E. Wisniewski, T. H. Shepard, E. A. Sersen, Brain growth in Down syndrome subjects 15 to 22 weeks of gestational age and birth to 60 months. *Clin. Neuropathol.* **9**, 181–190 (1990).
11. G. P. Reynolds, C. E. Warner, Amino acid neurotransmitter deficits in adult Down's syndrome brain tissue. *Neurosci. Lett.* **94**, 224–227 (1988).
12. D. Risser, G. Lubec, N. Cairns, M. Herrera-Marschitz, Excitatory amino acids and monoamines in parahippocampal gyrus and frontal cortical pole of adults with Down syndrome. *Life Sci.* **60**, 1231–1237 (1997).
13. S. J. Martin, P. D. Grimwood, R. G. Morris, Synaptic plasticity and memory: An evaluation of the hypothesis. *Annu. Rev. Neurosci.* **23**, 649–711 (2000).
14. T. V. Bliss, G. L. Collingridge, A synaptic model of memory: Long-term potentiation in the hippocampus. *Nature* **361**, 31–39 (1993).
15. R. J. Siarey, J. Stoll, S. I. Rapoport, Z. Galdzicki, Altered long-term potentiation in the young and old Ts65Dn mouse, a model for Down Syndrome. *Neuropharmacology* **36**, 1549–1554 (1997).
16. Z. Galdzicki, R. Siarey, R. Pearce, J. Stoll, S. I. Rapoport, On the cause of mental retardation in Down syndrome: Extrapolation from full and segmental trisomy 16 mouse models. *Brain Res. Brain Res. Rev.* **35**, 115–145 (2001).
17. P. Goelet, V. F. Castellucci, S. Schacher, E. R. Kandel, The long and the short of long–term memory—A molecular framework. *Nature* **322**, 419–422 (1986).
18. K. P. Scholz, J. H. Byrne, Intracellular injection of cAMP induces a long-term reduction of neuronal $K^+$ currents. *Science* **240**, 1664–1666 (1988).
19. P. K. Dash, B. Hochner, E. R. Kandel, Injection of the cAMP-responsive element into the nucleus of Aplysia sensory neurons blocks long-term facilitation. *Nature* **345**, 718–721 (1990).
20. M. Brunelli, V. Castellucci, E. R. Kandel, Synaptic facilitation and behavioral sensitization in Aplysia: Possible role of serotonin and cyclic AMP. *Science* **194**, 1178–1181 (1976).
21. D. Byers, R. L. Davis, J. A. Kiger Jr., Defect in cyclic AMP phosphodiesterase due to the dunce mutation of learning in Drosophila melanogaster. *Nature* **289**, 79–81 (1981).
22. B. Mayr, M. Montminy, Transcriptional regulation by the phosphorylation-dependent factor CREB. *Nat. Rev. Mol. Cell Biol.* **2**, 599–609 (2001).
23. M. Kikuchi, S. Morita, M. Wakamori, S. Sato, T. Uchikubo-Kamo, T. Suzuki, N. Dohmae, M. Shirouzu, T. Umehara, Epigenetic mechanisms to propagate histone acetylation by p300/CBP. *Nat. Commun.* **14**, 4103 (2023).
24. D. C. Bedford, P. K. Brindle, Is histone acetylation the most important physiological function for CBP and p300? *Aging* **4**, 247–255 (2012).
25. L. W. Yuan, J. E. Gambee, Histone acetylation by p300 is involved in CREB-mediated transcription on chromatin. *Biochim. Biophys. Acta* **1541**, 161–169 (2001).
26. M. Dierssen, I. F. Vallina, C. Baamonde, M. A. Lumbreras, C. Martínez-Cué, S. G. Calatayud, J. Flórez, Impaired cyclic AMP production in the hippocampus of a Down syndrome murine model. *Brain Res. Dev. Brain Res.* **95**, 122–124 (1996).

27. T. Collins, J. R. Stone, A. J. Williams, All in the family: The BTB/POZ, KRAB, and SCAN domains. *Mol. Cell. Biol.* **21**, 3609–3615 (2001).
28. O. Albagli, P. Dhordain, C. Deweindt, G. Lecocq, D. Leprince, The BTB/POZ domain: A new protein-protein interaction motif common to DNA- and actin-binding proteins. *Cell Growth Differ.* **6**, 1193–1198 (1995).
29. K. Takebayashi-Suzuki, M. Uchida, A. Suzuki, Zbtb21 is required for the anterior-posterior patterning of neural tissue in the early Xenopus embryo. *Biochem. Biophys. Res. Commun.* **630**, 190–197 (2022).
30. H. Hou, X. Wang, C. Yang, X. Cai, W. Lv, Y. Tu, A. Bao, Q. Wu, W. Zhao, J. Yao, Comparative genome and transcriptome integration studies reveal the mechanism of pectoral muscle development and function in pigeons. *Front. Genet.* **12**, 735795 (2021).
31. Y. Ding, D. Z. Yang, Y. N. Zhai, K. Xue, F. Xu, X. Y. Gu, S. M. Wang, Microarray expression profiling of long non-coding RNAs in epithelial ovarian cancer. *Oncol. Lett.* **14**, 2523–2530 (2017).
32. M. R. Sailani, P. Makrythanasis, A. Valsesia, F. A. Santoni, S. Deutsch, K. Popadin, C. Borel, E. Migliavacca, A. J. Sharp, G. D. Sail, The complex SNP and CNV genetic architecture of the increased risk of congenital heart defects in Down syndrome. *Genome Res.* **23**, 1410–1421 (2013).
33. H. S. Kaya-Okur, S. J. Wu, C. A. Codomo, E. S. Pledger, T. D. Bryson, J. G. Henikoff, K. Ahmad, S. Henikoff, CUT&Tag for efficient epigenomic profiling of small samples and single cells. *Nat. Commun.* **10**, 1930 (2019).
34. C. R. Palmer, C. S. Liu, W. J. Romanow, M. H. Lee, J. Chun, Altered cell and RNA isoform diversity in aging Down syndrome brains. *Proc. Natl. Acad. Sci. U.S.A.* **118**, e2114326118 (2021).
35. L. Zimmerman, U. Lendahl, M. Cunningham, R. McKay, B. Parr, B. Gavin, J. Mann, G. Vassileva, A. McMahon, Independent regulatory elements in the nestin gene direct transgene expression to neural stem cells or muscle precursors. *Neuron* **12**, 11–24 (1994).
36. N. C. Dubois, D. Hofmann, K. Kaloulis, J. Bishop, A. Trumpp, Nestin-Cre transgenic mouse line Nes-Cre1 mediates highly efficient Cre/loxP mediated recombination in the nervous system, kidney, and somite-derived tissues. *Genesis* **44**, 355–360 (2006).
37. L. A. Gabel, I. Marin, J. J. LoTurco, A. Che, C. Murphy, M. Manglani, S. Kass, Mutation of the dyslexia-associated gene Dcdc2 impairs LTM and visuo-spatial performance in mice. *Genes Brain Behav.* **10**, 868–875 (2011).
38. D. T. Truong, A. Che, A. R. Rendall, C. E. Szalkowski, J. J. LoTurco, A. M. Galaburda, R. Holly Fitch, Mutation of Dcdc2 in mice leads to impairments in auditory processing and memory ability. *Genes Brain Behav.* **13**, 802–811 (2014).
39. C. M. Pereira, E. Sattlegger, H. Y. Jiang, B. M. Longo, C. B. Jaqueta, A. G. Hinnebusch, R. C. Wek, L. E. Mello, B. A. Castilho, IMPACT, a protein preferentially expressed in the mouse brain, binds GCN1 and inhibits GCN2 activation. *J. Biol. Chem.* **280**, 28316–28323 (2005).
40. P. Yan, Z. Xue, D. Li, S. Ni, C. Wang, X. Jin, D. Zhou, X. Li, X. Zhao, X. Chen, W. Cui, D. Xu, W. Zhou, J. Zhang, Dysregulated CRTC1-BDNF signaling pathway in the hippocampus contributes to Aβ oligomer-induced long-term synaptic plasticity and memory impairment. *Exp. Neurol.* **345**, 113812 (2021).
41. S. Uchida, G. P. Shumyatsky, Epigenetic regulation of Fgf1 transcription by CRTC1 and memory enhancement. *Brain Res. Bull.* **141**, 3–12 (2018).
42. J. O. Korbel, T. Tirosh-Wagner, A. E. Urban, X. N. Chen, M. Kasowski, L. Dai, F. Grubert, C. Erdman, M. C. Gao, K. Lange, E. M. Sobel, G. M. Barlow, A. S. Aylsworth, N. J. Carpenter, R. D. Clark, M. Y. Cohen, E. Doran, T. Falik-Zaccai, S. O. Lewin, I. T. Lott, B. C. McGillivray, J. B. Moeschler, M. J. Pettenati, S. M. Pueschel, K. W. Rao, L. G. Shaffer, M. Shohat, A. J. Van Riper, D. Warburton, S. Weissman, M. B. Gerstein, M. Snyder, J. R. Korenberg, The genetic architecture of Down syndrome phenotypes revealed by high-resolution analysis of human segmental trisomies. *Proc. Natl. Acad. Sci. U.S.A.* **106**, 12031–12036 (2009).
43. S. Delhaye, B. Bardoni, Role of phosphodiesterases in the pathophysiology of neurodevelopmental disorders. *Mol. Psychiatry* **26**, 4570–4582 (2021).
44. K. Rutten, C. Lieben, L. Smits, A. Blokland, The PDE4 inhibitor rolipram reverses object memory impairment induced by acute tryptophan depletion in the rat. *Psychopharmacology* **192**, 275–282 (2007).
45. M. Tsuji, M. Ohshima, Y. Yamamoto, S. Saito, Y. Hattori, E. Tanaka, A. Taguchi, M. Ihara, Y. Ogawa, Cilostazol, a phosphodiesterase 3 inhibitor, moderately attenuates behaviors depending on sex in the Ts65Dn mouse model of down syndrome. *Front. Aging Neurosci.* **12**, 106 (2020).
46. E. A. Vitalis, J. L. Costantin, P. S. Tsai, H. Sakakibara, S. Paruthiyil, T. Iiri, J. F. Martini, M. Taga, A. L. Choi, A. C. Charles, R. I. Weiner, Role of the cAMP signaling pathway in the regulation of gonadotropin-releasing hormone secretion in GT1 cells. *Proc. Natl. Acad. Sci. U.S.A.* **97**, 1861–1866 (2000).
47. M. Manfredi-Lozano, V. Leysen, M. Adamo, I. Paiva, R. Rovera, J. M. Pignat, F. E. Timzoura, M. Candlish, S. Eddarkaoui, S. A. Malone, M. S. B. Silva, S. Trova, M. Imbernon, L. Decoster, L. Cotellessa, M. Tena-Sempere, M. Claret, A. Paoloni-Giacobino, D. Plassard, E. Paccou, N. Vionnet, J. Acierno, A. M. Maceski, A. Lutti, F. Pfrieger, S. Rasika, F. Santoni, U. Boehm, P. Ciofi, L. Buée, N. Haddjeri, A. L. Boutillier, J. Kuhle, A. Messina, B. Draganski, P. Giacobini, N. Pitteloud, V. Prevot, GnRH replacement rescues cognition in Down syndrome. *Science* **377**, eabq4515 (2022).
48. S. Larivière, G. Garrel, M. T. Robin, R. Counis, J. Cohen-Tannoudji, Differential mechanisms for PACAP and GnRH cAMP induction contribute to cross-talk between both hormones in the gonadotrope LbetaT2 cell line. *Ann. N. Y. Acad. Sci.* **1070**, 376–379 (2006).
49. J.-J. Fuentes, M. A. Pritchard, A. M. Planas, A. Bosch, I. Ferrer, X. Estivill, A new human gene from the Down syndrome critical region encodes a proline-rich protein highly expressed in fetal brain and heart. *Hum. Mol. Genet.* **4**, 1935–1944 (1995).
50. S. R. Seo, K. C. Chung, CREB activates proteasomal degradation of DSCR1/RCAN1. *FEBS Lett.* **582**, 1889–1893 (2008).
51. N. Y. Hu, Y. T. Chen, Q. Wang, W. Jie, Y. S. Liu, Q. L. You, Z. L. Li, X. W. Li, S. Reibel, F. W. Pfrieger, J. M. Yang, T. M. Gao, Expression patterns of inducible cre recombinase driven by differential astrocyte-specific promoters in transgenic mouse lines. *Neurosci. Bull.* **36**, 530–544 (2020).
52. F. Zeng, X. Ma, L. Zhu, Q. Xu, Y. Zeng, Y. Gao, G. Li, T. Guo, H. Zhang, X. Tang, Z. Wang, Z. Ye, L. Zheng, H. Zhang, Q. Zheng, K. Li, J. Lu, X. Qi, H. Luo, X. Zhang, Z. Wang, Y. Zhou, Y. Yao, R. Ke, Y. Zhou, Y. Liu, H. Sun, T. Huang, Z. Shao, H. Xu, X. Wang, The deubiquitinase USP6 affects memory and synaptic plasticity through modulating NMDA receptor stability. *PLOS Biol.* **17**, e3000525 (2019).
53. D. W. Zhang, J. Shao, J. Lin, N. Zhang, B. J. Lu, S. C. Lin, M. Q. Dong, J. Han, RIP3, an energy metabolism regulator that switches TNF-induced cell death from apoptosis to necrosis. *Science* **325**, 332–336 (2009).
54. W. Chen, J. Wu, L. Li, Z. Zhang, J. Ren, Y. Liang, F. Chen, C. Yang, Z. Zhou, S. S. Su, X. Zheng, Z. Zhang, C. Q. Zhong, H. Wan, M. Xiao, X. Lin, X. H. Feng, J. Han, Ppm1b negatively regulates necroptosis through dephosphorylating Rip3. *Nat. Cell Biol.* **17**, 434–444 (2015).
55. W. J. Zhang, X. N. Wu, T. T. Shi, H. T. Xu, J. Yi, H. F. Shen, M. F. Huang, X. Y. Shu, F. F. Wang, B. L. Peng, R. Q. Xiao, W. W. Gao, J. C. Ding, W. Liu, Regulation of transcription factor yin yang 1 by SET7/9-mediated lysine methylation. *Sci. Rep.* **6**, 21718 (2016).
56. X. N. Wu, T. T. Shi, Y. H. He, F. F. Wang, R. Sang, J. C. Ding, W. J. Zhang, X. Y. Shu, H. F. Shen, J. Yi, X. Gao, W. Liu, Methylation of transcription factor YY2 regulates its transcriptional activity and cell proliferation. *Cell Discov.* **3**, 17035 (2017).
57. H. Zhang, Y. Hong, W. Yang, R. Wang, T. Yao, J. Wang, K. Liu, H. Yuan, C. Xu, Y. Zhou, G. Li, L. Zhang, H. Luo, X. Zhang, D. Du, H. Sun, Q. Zheng, Y. W. Zhang, Y. Zhao, Y. Zhou, H. Xu, X. Wang, SNX14 deficiency-induced defective axonal mitochondrial transport in Purkinje cells underlies cerebellar ataxia and can be reversed by valproate. *Natl. Sci. Rev.* **8**, nwab024 (2021).
58. Z. H. Yang, X. N. Wu, P. He, X. Wang, J. Wu, T. Ai, C. Q. Zhong, X. Wu, Y. Cong, R. Zhu, H. Li, Z. Y. Cai, W. Mo, J. Han, A non-canonical PDK1-RSK signal diminishes pro-caspase-8-mediated necroptosis blockade. *Mol. Cell* **80**, 296–310.e6 (2020).
59. S. Shultz, T. Worzella, A. Gallagher, J. Shieh, S. Goueli, K. Hsiao, J. Vidugiriene, Miniaturized GPCR signaling studies in 1536-well format. *J. Biomol. Tech.* **19**, 267–274 (2008).
60. H. M. T. Choi, M. Schwarzkopf, M. E. Fornace, A. Acharya, G. Artavanis, J. Stegmaier, A. Cunha, N. A. Pierce, Third-generation in situ hybridization chain reaction: Multiplexed, quantitative, sensitive, versatile, robust. *Development* **145**, dev165753 (2018).


**Acknowledgments:** We thank Y. Gao, H. Fang, C. Xu, H. Zhang, Q. Zheng, Y. Hong, G. Li, X. Gao, T. Teng, and L. Li for technical help. We also thank the Consultant Program of Medical Statistics, National Institute for Data Science in Health and Medicine, School of Medicine, Xiamen University for analysis assistance. **Funding:** This work was supported by the National Key R&D Program of China (2020YFA0803500 to J.H. and 2021YFA1101401 to X.W.), the National Natural Science Foundation of China (82388201 to J.H. and U21A20358 and 82325018 to X.W.), the CAMS Innovation Fund for Medical Science (2019-I2M-5-062 to J.H.), Fujian province central to local science and technology development special program (no. 2022 L3079 to J.H.), and Fu-Xia-Quan Zi-Chuang district cooperation program (no. 3502ZCQXT2022003 to J.H.). **Author contributions:** J.H. conceptualized and designed the project. J.H. and X.W. conceived the experiments and supervised the study. M.Q. generated DNA constructs and ZBTB21 KO cells used in this study. M.Q. performed quantitative MS and relevant validation on cells. Q.H. conducted most of the behavioral tests and analyzed the data. Q.H. also carried out electrophysiological experiments, RNA-seq, CUT&Tag-seq, and analyzed the data. J.H. and X.W. assisted with all data analysis and provided helpful discussions and methodology. J.H., X.W., and Q.H. wrote most of the original draft. J.H., X.W., Q.H., and M.Q. participated in writing, reviewing, editing, and formal analysis. J.H. and X.W. acquired the funding. All authors reviewed the manuscript. **Competing interests:** The authors declare that they have no competing interests. **Data and materials availability:** The raw MS data have been deposited to the ProteomeXchange Consortium via the iProX partner repository with the dataset identifier PXD040133. The bulk RNA-seq and CUT&Tag-seq data were deposited in the CNGB Sequence Archive of the China National GeneBank Database with the accession numbers CNP0005186, CNP0005223, and CNP0005215. All data needed to evaluate the conclusions in the paper are present in the paper and/or the Supplementary Materials.

Submitted 4 November 2023
Accepted 30 May 2024
Published 3 July 2024
10.1126/sciadv.adm7373